DOI: 10.26599/FSHW.2026.9251269

Contents lists available at SciOpen

Food Science and Human Wellness

journal homepage: https://www.sciopen.com/journal/2097-0765

China Food Publishing Co.

Dietary Tamarixetin Alleviates Copper Overload-Induced Hepatotoxicity via Copper Chelation, Cuproptosis Inhibition, and Gut-Liver Axis Modulation: A Study on Flavonoid-Metal Interactions

Hao Wang[a, †], Jinsong Zhang[b, †], Meng Zhou[a, †], Wen Li[c], Leyi Chu[b], Xiaofeng Ruan [b], Tianling Pan[b], Yue Li[b], Jinzhi Ma[b], Peng Xiao[b, *], Hong Gao[b, c, *]

[a] *College of Food Science and Technology, Yunnan Agricultural University, Kunming 650201, China*

[b] *College of Veterinary Medicine, Yunnan Agricultural University, Kunming 650201, China*

[c] *Faculty of Animal Science and Technology, Yunnan Agricultural University, Kunming 650201, China*

ABSTRACT: Excessive dietary copper is a nutritional toxicant that disrupts homeostasis and provokes liver injury; yet the role of cuproptosis (copper-dependent cell death) is not fully defined. Tamarixetin (TAM), a food-derived flavonoid with copper-chelating and antioxidant capacity, was evaluated as a protective bioactive. We demonstrate that copper overload drives hepatotoxicity predominantly through cuproptosis. TAM lowered labile copper and activated the nuclear receptor NR1I2, thereby upregulating lipoic acid synthase (LIAS) to inhibit cuproptosis and restore tricarboxylic acid cycle function. NR1I2 overexpression phenocopied TAM-mediated protection, confirming the NR1I2–LIAS axis. TAM also reshaped the gut microbiota, enriching Lactobacillus and, via the gut–liver axis, suppressing NF-κB–mediated hepatic inflammation. Overall, these findings reveal a flavonoid–metal interaction-based defense mechanism and support TAM as a functional ingredient or nutraceutical to mitigate high dietary copper exposure.

Keywords: Nutritional toxicant; Copper overload; Tamarixetin; Hepatotoxicity; Cuproptosis; NR1I2-LIAS Pathway; Gut-Liver Axis

1. Introduction

Copper is an essential trace element and a core cofactor of cytochrome c oxidase and superoxide dismutase (SOD1) [1, 2]. It plays a critical role in cellular energy metabolism and redox homeostasis. However, excess copper can generate reactive oxygen species (ROS) via Fenton-like reactions, leading to oxidative damage [3]. Chronic ingestion of high-copper diets—commonly from specific organ meats, shellfish, or contaminated water sources—can result in systemic accumulation, particularly in patients with genetic copper metabolism disorders such as Wilson disease or Menkes disease [4-6]. This dietary or

† Hao Wang, Jinsong Zhang, and Meng Zhou contributed equally to this work.
***Corresponding Author**
Hong Gao gaohongping@163.com (H.Gao)
Peng Xiao aipengpengpiao@163.com (P.Xiao)

Received 24 February 2026
Received in revised from 6 April 2026
Accepted 21 April 2026

environmental copper overload induces mitochondrial dysfunction, lipid peroxidation, and oxidative stress [7-9], presenting a significant challenge in food safety and nutritional toxicology.

A recently identified modality of programmed cell death, dependent on copper and termed cuproptosis, offers a novel mechanistic perspective on copper-induced cytotoxicity[10, 11]. Unlike apoptosis, pyroptosis, or ferroptosis, this form of cell death is driven by excess Cu^{2+} directly binding to lipoic acid-modified enzymes in the TCA cycle, such as dihydrolipoamide S-acetyltransferase (DLAT). This binding induces abnormal oligomerization and aggregation of these enzymes, triggering mitochondrial proteotoxic stress and concomitant loss of Fe-S cluster proteins [12-14]. Notably, FDX1 reduces Cu^{2+} to the more toxic Cu^{+}, thereby accelerating copper binding to lipoylated proteins [15-17]. Conversely, LIAS (lipoic acid synthase), which is essential for protein lipoylation, plays a protective role: downregulation of LIAS undermines lipoylation stability and exacerbates cuproptosis, whereas maintaining LIAS levels markedly attenuates it [18, 19]. Cuproptosis depends on functional mitochondrial respiration and the TCA cycle, and is characterized by a disrupted TCA cycle with accumulation of pyruvate and α-ketoglutarate, along with depletion of succinate [18]. Therefore, identifying bioactive food components that can modulate these pathways offers a promising strategy to mitigate metal toxicity.

Tamarixetin (TAM) is a quercetin metabolite and natural flavonoid known for its potent anti-inflammatory and metal-chelating properties [20, 21]. It is present in plants such as Tamarix species, Blumea balsamifera (Ai-na-xiang), and Ginkgo biloba [22, 23] Its catechol structure enables efficient chelation of free copper ions [21], making TAM a promising natural agent to counteract copper overload–related toxicity. Previous studies have shown that TAM can enhance cell viability and reduce apoptosis by inhibiting the NFAT/AKT pathway [24], and attenuate oxidative stress and pyroptosis by activating the Nrf2 pathway while inhibiting NF-κB activation [25] Additionally, TAM has been reported to upregulate IL-10 (interleukin-10) expression and decrease LPS (lipopolysaccharide)-induced release of pro-inflammatory cytokines, thereby exerting anti-inflammatory effects [26]. In models of pollutant-induced liver injury, TAM demonstrated antioxidant protection and ameliorated liver damage via the Nrf2/Keap1 pathway [27]. Therefore, although TAM's antioxidant and anti-inflammatory benefits are well documented, its protective mechanism remains incompletely understood — in particular, whether its copper-sequestering ability can inhibit cuproptosis has not been systematically investigated.

In this study, we identified a novel regulatory axis in which TAM suppresses cuproptosis by upregulating LIAS expression via activation of the nuclear receptor NR1I2. Moreover, TAM beneficially increases the abundance of *Lactobacillus* and, through the gut-liver axis, attenuates NF-κB mediated hepatic inflammation. These findings clarify the pivotal role of cuproptosis in copper overload–induced liver injury and suggest innovative dietary intervention strategies. In particular, TAM's multi-faceted actions highlight the potential of natural dietary flavonoids as functional food components or additives to help protect against copper-associated liver damage.

2. Materials and methods

2.1. Animal experiments

C57BL/6 mice (♂, 7-8 weeks old) were obtained from the Institute of Medical Biology, Chinese Academy of Medical Sciences, and maintained under specific pathogen-free (SPF) conditions at Yunnan Agricultural University. Mice were housed on a 12-h light/dark cycle at 25 ± 2 °C and 40 ± 10% relative humidity, with ad libitum access to standard chow and water. Forty mice were randomized into four groups (n = 10 per group): control (Con), $CuSO_4$-induced copper overload ($CuSO_4$), tamarixetin intervention (TAM), and tetrathiomolybdate comparator (TTM). For 21 consecutive days, mice in the $CuSO_4$ and TAM groups received $CuSO_4$ (40 mg·kg^{-1}) once daily by oral gavage [28]. Mice in the TAM group also received tamarixetin (20 mg·kg^{-1}) by oral gavage [29]. Where included as a copper-chelating comparator to benchmark cuproptosis-related effects, mice in the TTM group received tetrathiomolybdate (30 mg·kg^{-1}) by oral gavage [29]. Control mice received vehicle only. Twenty-four hours after the final dose, mice were euthanized and blood and liver samples were collected for histological, biochemical, and molecular analyses. Hepatomegaly was quantified as the liver index (liver weight/body weight × 100%). All procedures were approved by the Animal Ethics Committee of Yunnan Agricultural University (No. 202303006) and conducted in accordance with the ARRIVE guidelines.

2.2. Cell culture and treatment

HepG2 cells (ATCC HB-8065) were cultured in DMEM supplemented with 10% FBS and 1% penicillin-streptomycin at 37 °C in a humidified atmosphere with 5% CO_2. To establish a copper-overload model, cells were assigned to three groups: control (vehicle), $CuSO_4$ (200 μM) [24], and $CuSO_4$ + TAM (co-treatment). Cells in the $CuSO_4$ + TAM group were co-treated with TAM at the optimal concentration determined by preliminary dose-response experiments for the indicated times. After the treatments, cells and culture supernatants were collected for downstream assays.

For studies of cuproptosis inhibition, HepG2 cells were first exposed to the cuproptosis inducer Elesclomol-Cu (1:1, 40 nM [30]) for the indicated time, and were then treated with TAM (post-induction treatment).

2.3. Cell viability assays

Cell viability was measured using the CCK-8 Kit (Yeasen, #40203ES) according to the manufacturer's instructions. To determine the optimal concentration of TAM, cells were treated in basal medium with TAM at 1, 5, 10, 25, 50, 100, and 200 μM. To interrogate the mechanism of cell death, cells were pretreated with one of the following inhibitors: TTM, (20 μM; Sigma-Aldrich #323446), Z-VAD-FMK (30 μM; Selleck Chemicals #S7023), ferrostatin-1 (Fer-1, 10 μM; Selleck Chemicals #S7243), necrostatin-1 (Nec-1, 20 μM; Enzo #BML-AP309), or 3-methyladenine (3-MA, 5 mM; MedChemExpress #HY-19312) [30]. After inhibitor pretreatment, cells were co-incubated with $CuSO_4$ (200 μM) and the selected concentration of TAM for the indicated time, and cell viability was then assessed by the CCK-8 assay. Cytotoxicity was evaluated by measuring lactate dehydrogenase release using the LDH Cytotoxicity Assay Kit (Yeasen, #40209ES).

2.4. Tissue Staining and Microscopy:

Liver tissue was sectioned at 5 μm from paraffin-embedded blocks, deparaffinized, rehydrated, and stained with H&E. H&E-stained sections were examined under an Olympus BX53 light microscope.

For immunohistochemistry (IHC), deparaffinized sections underwent antigen retrieval in citrate buffer and endogenous peroxidase activity was quenched with H_2O_2. After blocking with 5% BSA, sections were incubated with anti-IL-1β primary antibody, washed with PBS, and incubated with the corresponding secondary antibody. Immunoreactivity was developed with DAB, counterstained with hematoxylin, and observed using an Olympus BX53 light microscope. For immunofluorescence (IF), frozen sections were prepared, blocked with 5% BSA as above, and incubated with anti-TNF-α primary antibody. After washing, sections were incubated with fluorophore-conjugated secondary antibodies, and nuclei were counterstained with DAPI. Fluorescence images were acquired with a fluorescence microscope.

2.5. Biochemical analysis in the plasma and tissue

Following euthanasia, blood was collected and centrifuged at 1,200 × g for 10 min at 4 °C to obtain plasma. Tissue homogenates were prepared by grinding tissues in PBS. The activities of aspartate aminotransferase (AST; kit #C010 2 1), alanine aminotransferase (ALT; kit #C009 2 1), alkaline phosphatase (ALP; kit #A059 2 2), total bilirubin (TBIL; kit #C019 1 1), glutamate dehydrogenase (GLDH; kit #E BC K759 M), and adenosine triphosphate (ATP; kit #E BC K157 S) were measured in plasma or tissue homogenates using commercial assay kits (Nanjing Jiancheng Bioengineering Institute or Elabscience) according to the manufacturers' instructions.

2.6. Inductively coupled plasma mass spectrometry

To measure copper content, cell pellets and liver tissues were digested and analyzed by ICP-MS. Cell pellets were digested in concentrated nitric acid at 65 °C for 1 hour, then diluted with ultrapure water. Liver tissue samples (0.1 g) were placed in PTFE digestion vessels, moistened with 0.5 mL distilled water, and digested sequentially with 5 mL concentrated nitric acid for 1 hour and 1 mL hydrogen peroxide. After digestion, an indium internal standard (50 μL of 100 ng/mL) was added to each sample, and copper content was measured using a NexION 1000G ICP-MS system.

2.7. Assessment of hepatic energy metabolism

To evaluate hepatic energy homeostasis, pyruvate dehydrogenase (PDH) activity in was measured using a colorimetric assay kit (Elabscience, #EBC-K650M) following the manufacturer’s instructions. Key TCA cycle intermediates pyruvate (#EBC-F058), citrate (#EBC-K351M), α-ketoglutarate (#EBC-F047), and malate (#EBC-K905M) were quantified using their respective colorimetric kits (Elabscience).

2.8. RNA-seq

Total RNA was extracted from cell samples. RNA integrity was evaluated using an Agilent 2100 Bioanalyzer. Sequencing libraries were prepared with the NEBNext Ultra II RNA Library Prep Kit and sequenced on an Illumina NovaSeq 6000 platform (sequencing performed by Aptbiotech). Differential

expression analysis was performed with DESeq2. Genes with |log2 fold change| ≥ 1.3 and $P < 0.05$ were considered differentially expressed. Differentially expressed genes (DEGs) were subjected to KEGG pathway enrichment analysis and Gene Ontology (GO) functional annotation.

2.9. Reverse transcription quantitative polymerase chain reaction (RT-qPCR)

For RT-qPCR, total RNA from mouse liver and HepG2 cells was isolated using AG RNAex Pro Reagent (Accurate Bio, #AG21102). Reverse transcription was performed with the Hifair® III First Strand cDNA Synthesis SuperMix (Yeasen, #40203ES) according to the manufacturer's protocol, which includes a genomic DNA removal step. qPCR was carried out on the synthesized cDNA using Hieff UNICON® Universal Blue qPCR SYBR Green Master Mix (Yeasen, #11184ES) with GAPDH as the internal reference gene. Relative expression levels were calculated using the $2^{-\Delta\Delta Ct}$ method. Primer sequences were obtained from the PrimerBank database [31, 32].

2.10. 16S rRNA gut microbiome sequencing

Fecal microbial DNA was extracted from mice using the QIAamp DNA Mini Kit. Library preparation and 16S rRNA gene sequencing were performed by Biomarker Technologies Co., Ltd. (Shanghai, China). Sequencing data were analyzed for alpha and beta diversity. Differentially abundant taxa were identified using LEfSe (LDA score > 4, $P < 0.05$), and functional potential was predicted against the KEGG database via PICRUSt.

2.11. Construction and transfection of overexpression plasmids

To overexpress NR1I2, full-length human NR1I2 cDNA was amplified from HepG2 cells and cloned into the pEGFP-C3 vector (Clontech) at EcoRI/KpnI sites, generating the pEGFP-C3-NR1I2 construct. For transfection, 2 μg of the plasmid DNA was mixed with Engreen Transfection Reagent (Engreen Biosystem, #98668) and introduced into target cells by electroporation using a Gene Pulser Xcell system (Bio-Rad) set to 250 V and 950 μF.

2.12. Dual luciferase reporter gene assay

A fragment of the LIAS promoter (pLIAS) was synthesized (Sangon Biotech) and cloned into the pGL3 Basic vector (Addgene #212936) to create the pGL3-pLIAS reporter. HEK293T cells were co-transfected with the pGL3-pLIAS plasmid, the pEGFP-C3-NR1I2 construct, and the pRL-TK plasmid (Beyotime, #D2760) as an internal control. After 48 hours, firefly and Renilla luciferase activities were measured using the Dual Luciferase® Reporter Assay System (Promega, #E1910).

2.13. Western blot

Proteins were extracted from cells or tissues using RIPA buffer and quantified by BCA assay. Equal amounts of protein were separated by 12% PAGE and transferred onto PVDF membranes. Membranes were blocked with 5% BSA for 1 hour at room temperature and then incubated overnight at 4 °C with the following primary antibodies: FDX1 (Proteintech, 67912-1-Ig), ACO2 (Abcam, ab129069), SDHB (Abcam, ab178423), NR1I2 (Proteintech, 67912-1-Ig), DLAT (Thermo Fisher, 120279), LIAS (Proteintech,

11577-1-AP), and HSP70 (Proteintech, 66183-1-Ig). After washing with TBST, membranes were incubated with appropriate secondary antibodies for 1.5 hours at room temperature. Protein bands were visualized by enhanced chemiluminescence. GAPDH (Proteintech, 60004-1-AP) or β-actin (Proteintech, 66009-1-Ig) served as loading controls.

2.14. Detection of oxidative stress-related indicators

Oxidative stress markers were measured using commercial kits following the manufacturers' instructions: lipid peroxides (LPO; Nanjing Jiancheng Bioengineering Institute, #A106-1-2), glutathione peroxidase (GSH-Px; Nanjing Jiancheng, #A005-1-2), malondialdehyde (MDA; Boxbio, #AKFA013M), superoxide dismutase (SOD; Boxbio, #AKAO001M), and catalase (CAT; Boxbio, #AKAO003M).

2.15. Intracellular ROS Measurement

Intracellular ROS levels were quantified using a commercial ROS Assay Kit (Boxbio, #AKCE002-2) following the manufacturer's instructions. For fluorescence imaging, cells cultured on coverslips were incubated with 15 μM DHE at 37 °C for 30 minutes in the dark. Following two washes with PBS, fluorescence images were acquired using a fluorescence microscope.

2.16. Analysis of TAM Core Targets

The chemical structure of tamarixetin (PubChem CID: 5281699) was retrieved from PubChem. Potential targets of TAM were predicted using GeneCards, the CTD, BATMAN-TCM, and SwissTargetPrediction. Overlapping targets from these databases were identified through intersection analysis and visualized using UpSet and Venn diagrams. A set of cuproptosis-related genes (DPYD, DLAT, LIAS, DLD, LIPT1, PDHA1, PDHB) was compiled from the literature [30]. Transcription factors potentially co-regulating these genes were predicted using CHEA3[33], and overlapping candidates between the predicted transcription factors and TAM's targets were determined.

2.17. Molecular docking

The crystal structure of human NR1I2 (PDB ID: 9FZJ) was obtained from the RCSB PDB, and the 3D structure of TAM was retrieved from PubChem. Protein-ligand docking was performed using CB-Dock2 (https://cadd.labshare.cn/cb-dock2/php/index.php),, and binding energies below -5 kcal/mol were considered indicative of stable interactions [34]. Transcription factor binding sites in the LIAS promoter were predicted using JASPAR (https://jaspar.elixir.no/). Protein-DNA complex models were generated using AlphaFold3 (https://jaspar.elixir.no/) and evaluated based on the predicted TM score (pTM > 0.5) and interchain pTM score (ipTM > 0.8).

2.18. Statistical Analysis

All experiments were conducted with at least three biological replicates. Data are presented as mean ± SEM. Statistical comparisons were performed using Student's t-test or two-way ANOVA, with $P < 0.05$ considered statistically significant.

3. Result

3.1. TAM Chelates Copper to Alleviate Hepatotoxicity and Oxidative Stress Induced by High Copper Exposure

To investigate the effects of TAM on liver injury induced by high copper exposure, we established a $CuSO_4$-exposed mouse model and administered TAM intervention (Figure 1A). The results demonstrated that high copper exposure significantly impaired liver function, as indicated by elevated serum levels of AST, ALT, ALP, and TBIL. TAM treatment markedly attenuated these increases (Figure 1B-E). Furthermore, high copper exposure reduced liver mass, which was restored to near-normal levels after TAM treatment (Figure 1F). Histopathological analysis revealed that TAM alleviated copper overload-induced hepatocyte necrosis and disruption of hepatic cord structure (Figure 1G). Given TAM's strong copper-chelating ability [21], we measured hepatic copper content and found that TAM significantly reduced copper accumulation induced by high copper exposure (Figure 1H), consistent with its chelation activity. Since copper overload is known to trigger oxidative stress and subsequent tissue damage [35], we also examined oxidative stress-related indicators. TAM was found to inhibit copper-induced oxidative damage, significantly lowering MDA, SOD, and LPO levels, while increasing CAT and GSH-Px activities (Figure 1I). Together, these results demonstrate that TAM significantly mitigates copper-induced hepatotoxicity and oxidative stress through chelation of excess copper ions.

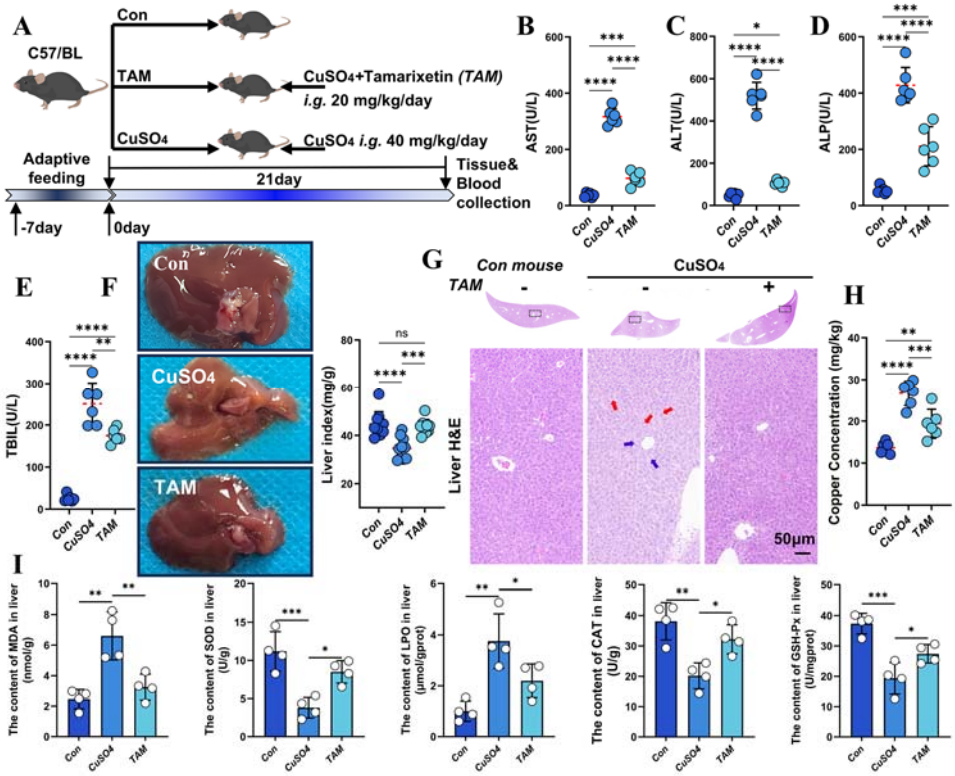


Figure 1. TAM chelation of copper alleviates copper-overload-induced hepatotoxicity and oxidative stress. (A) Schematic of the high-copper diet mouse model experimental design; (B-E) serum levels of (B) AST, (C) ALT, (D) ALP and (E) TBIL in mice (n = 6); (F) gross appearance of livers and liver index (n = 10); (G) H&E histopathological examination of liver tissue (scale bar: 50 μm; red arrows-hepatocyte death [loss of nuclei], blue arrows-hepatic cord architecture); (H) hepatic copper content measured by ICP-MS in each group (n = 6); (I) hepatic oxidative stress markers: MDA, SOD, LPO, CAT and GSH-Px (n = 4). Data are presented as mean ± SEM. (two-way ANOVA). * $P < 0.05$, ** $P < 0.01$, *** $P < 0.001$, **** $P < 0.0001$.

3.2. TAM Alleviates Cuproptosis Induced by High Copper Exposure

Given the protective effects of TAM on the liver, we established a high copper exposure model using $CuSO_4$ in HepG2 cells and applied TAM intervention (Figure 2A). First, a non-toxic concentration of TAM (100 μM) was determined for subsequent experiments (Figure 2B). High copper exposure induced cell death and increased LDH release, both of which were significantly mitigated by TAM treatment (Figure 2C-D). Intracellular copper measurement further showed that $CuSO_4$ led to substantial copper accumulation, while TAM effectively reduced intracellular copper levels (Figure 2E).

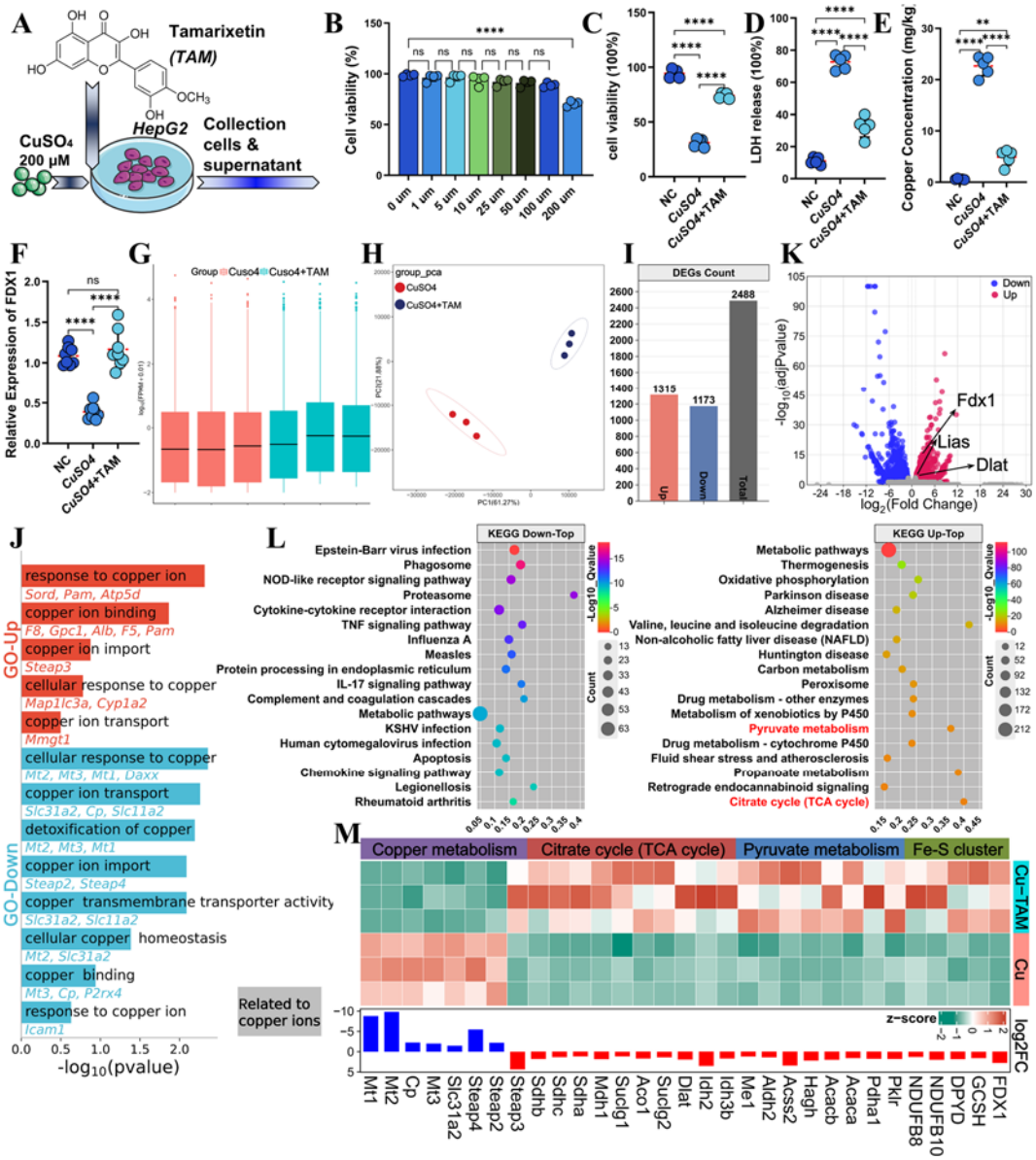


Figure 2. Transcriptomic analysis of the high-copper exposure cell model. (A) Experimental design for HepG2 cells exposed to high copper and treated with varying concentrations of TAM; (B) cell survival after different concentrations of TAM treatment (n = 4); (C-D) cell viability by CCK-8 assay (C) and LDH release rate (D) (n = 4); (E) cellular copper content measured by ICP-MS (n = 4); (F) qRT-PCR detection of *FDX1* mRNA expression (n = 8); (G) boxplots of gene expression FPKM values for each group; (H) PCA showing transcriptomic differences among samples; (I) statistics of DEGs between groups; (J) GO functional enrichment analysis of copper-ion-metabolism-related differential genes; (K) volcano plot of differential genes: red denotes upregulated genes, with genes related to the cuproptosis highlighted; (L) KEGG pathway enrichment analysis of differential genes between high-copper and TAM intervention groups (top pathways include TCA cycle, pyruvate metabolism, etc.); (M) hierarchical clustering heatmap of differential genes, showing expression patterns of genes related to TCA cycle, pyruvate metabolism, and Fe-S cluster assembly. Data are presented as mean ± SEM. (two-way ANOVA). **** $P < 0.0001$。

Since elevated copper levels under high copper exposure have been documented in both liver and cells, we examined the expression of FDX1, a key regulator of cuproptosis [30, 36]. $CuSO_4$ significantly decreased *FDX1* mRNA levels, and this reduction was reversed by TAM (Figure 2F). We then performed RNA-seq on cells subjected to high copper exposure with or without TAM. The FPKM distribution boxplot illustrated transcript abundance across samples (Figure 2G), and PCA showed clear separation between the experimental groups (Figure 2H). Differential expression analysis identified 2488 DEGs, including 1315 up-regulated and 1173 down-regulated genes. GO enrichment analysis indicated that TAM down-regulated multiple biological processes related to copper metabolism, such as reduced expression of copper transporters SLC31A2 and SLC11A2 (Figure 2J). Although FDX1, LIAS, and DLAT are recognized as positive regulators of cuproptosis, their downregulation during the progression of cuproptosis can impair protein lipoylation and tricarboxylic acid cycle function, thereby increasing cellular vulnerability to copper-induced death [30]. We noted that TAM up-regulated these key cuproptosis regulators, as shown in the volcano plot (Figure 2K). KEGG analysis revealed that high copper exposure activated cuproptosis-related pathways including the TCA cycle and pyruvate metabolism. These pathways were significantly enriched among genes up-regulated by TAM. Moreover, TAM up-regulated genes encoding Fe-S cluster proteins (e.g., *FDX1*, *NDUFB8*) and key TCA cycle enzymes (e.g., *DLAT*, *ACO2*, *SDHB*), while down-regulating genes involved in copper metabolism (e.g., *Steap2/3*) (Figure 2M). These findings suggest that cuproptosis contributes to hepatotoxicity induced by high copper exposure.

To further verify that high copper exposure triggers cuproptosis, we inhibited other programmed cell death pathways-pyroptosis, ferroptosis, necroptosis, and autophagy-or applied the copper chelator TTM. Only TTM alleviated copper-induced damage, and TAM showed a comparable protective effect (Figure 3A). We then analyzed cuproptosis-related protein expression. High copper exposure resulted in loss of Fe-S cluster proteins and suppressed DLAT aggregation, observable within 3 hours (Figure 3B-C). qPCR confirmed that $CuSO_4$ significantly decreased the mRNA levels of cuproptosis-related genes, including *FDX1*, *DLAT*, *LIAS*, *NDUFB8*, *ACO2*, *SDHB*, and *TOMM20*, while increasing *HSP70* mRNA expression. TAM treatment reversed these changes and partially restored their expression levels (Figure 2F, 3D-J). Western blotting further demonstrated that TAM inhibited the loss of Fe-S cluster proteins and prevented DLAT aggregation induced by $CuSO_4$ (Figure 3K-L). To specifically assess TAM's inhibitory effect on cuproptosis, we treated cells with the cuproptosis inducer ES-Cu along with TAM (Figure 3M). TAM reversed ES-Cu-induced cuproptosis and LDH release (Figure 3N-O), and inhibited aggregation of DLAT, a key marker of cuproptosis (Figure 3P-Q). Together, these results demonstrate that cuproptosis contributes to high copper-induced cell death, and that TAM effectively attenuates this process.

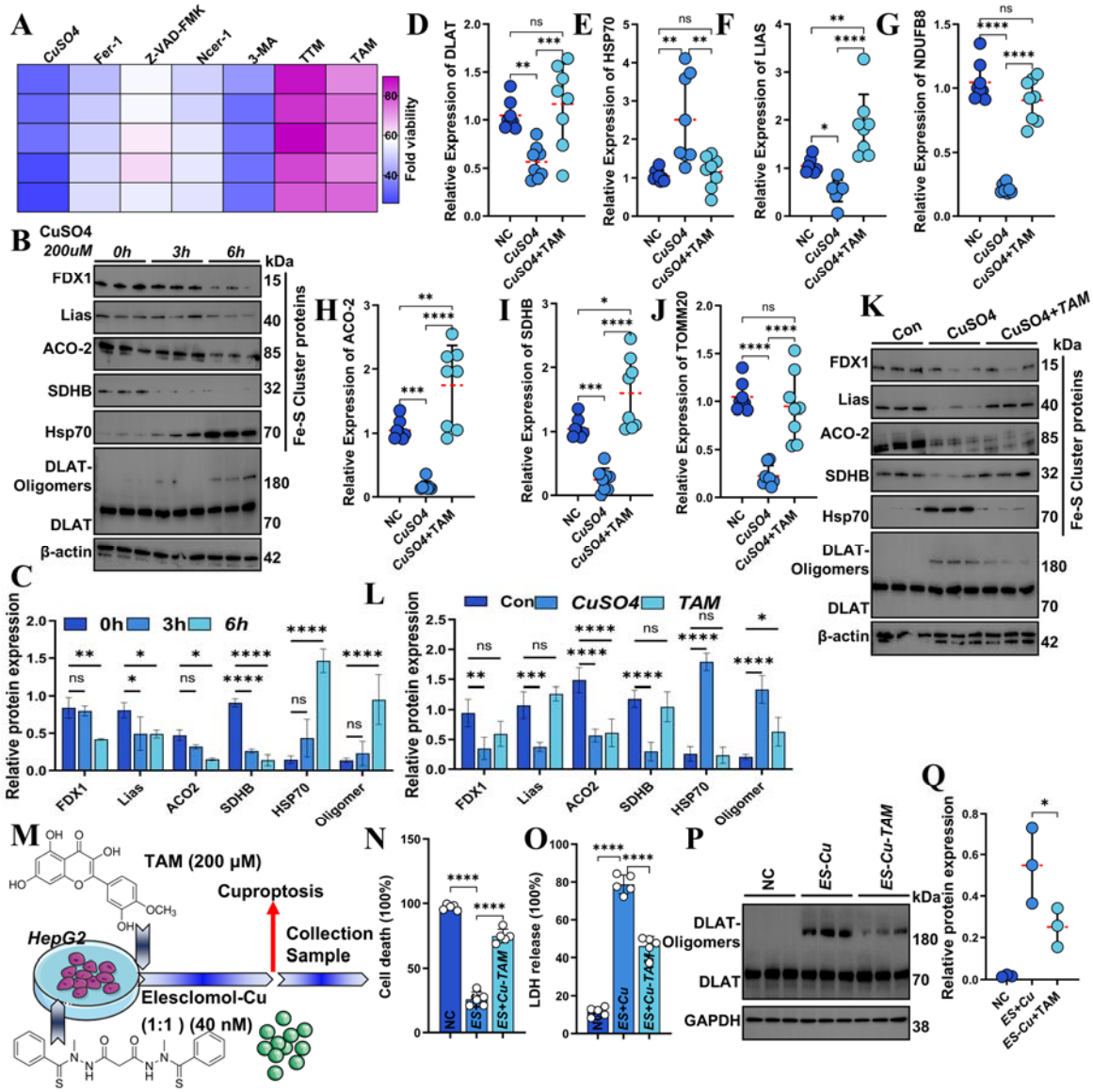


Figure 3. TAM alleviates copper-overload-induced cuproptosis. (A) HepG2 cells were pretreated with TTM, TAM, Z-VAD-FMK, Ferrostatin-1, Necrostatin-1 and 3-MA, respectively, followed by high-copper exposure for 8 h; cell viability was measured by CCK-8 and displayed as a heatmap (n = 5); (B-C) Western blot detection of Fe-S cluster proteins, HSP70 and DLAT oligomerization levels in HepG2 cells at different time points after high-copper exposure; (D-J) qRT-PCR measurement of cuproptosis-related gene mRNA expression in HepG2 cells 8 h after various treatments, including *DLAT*, *HSP70*, *LIAS*, *NDUFB8*, *ACO-2*, *SDHB* and *TOMM20* (n = 8); (K-L) Western blot detection of Fe-S cluster proteins, HSP70 and DLAT oligomerization levels after high-copper exposure and TAM intervention; (M) schematic of the cellular cuproptosis model experiment: HepG2 cells treated with Elesclomol-Cu (1:1, 40 nM) to establish a cuproptosis model, followed by TAM intervention; (N-O) cell viability by CCK-8 (N) and LDH release rate (O) (n = 4); (P-Q) Western blot analysis of DLAT oligomerization levels in the cuproptosis model and after TAM intervention. Data are presented as mean ± SEM. (two-way ANOVA). * $P < 0.05$, ** $P < 0.01$, *** $P < 0.001$, **** $P < 0.0001$。

3.3. TAM Alleviates High Copper Exposure-Induced Liver Metabolic Disorders and Hepatotoxicity by Inhibiting Cuproptosis

Following the confirmation of cuproptosis involvement in high copper-induced cell death, we further assessed its role in copper-induced hepatotoxicity. qPCR results revealed that high copper exposure significantly decreased mRNA levels of key cuproptosis regulatory genes (including *FDX1*, *TOMM20, SDHB*, *LIAS*, *ACO2*, and *DLAT*) in the liver. These reductions were reversed by the cuproptosis inhibitor TTM, and TAM treatment produced similar effects (Figure 4A). Immunoblot analysis further confirmed that

TAM significantly alleviated the loss of Fe-S cluster proteins and inhibited DLAT aggregation induced by $CuSO_4$ exposure (Figure 4B-D). Inhibition of the TCA cycle is a central metabolic alteration in cuproptosis [30]. Accordingly, we analyzed TCA cycle metabolites. High copper treatment resulted in significant accumulation of pyruvate and citrate, along with marked decreases in α-ketoglutarate and malate levels in the liver. TAM treatment reversed these metabolic alterations (Figure 4E). Given that DLAT a core component of the pyruvate dehydrogenase complex that requires lipoylation for enzymatic activity tends to aggregate during cuproptosis [30], we measured pyruvate dehydrogenase activity in the liver. The results indicated that high copper exposure significantly suppressed pyruvate dehydrogenase activity, while TAM markedly restored its function (Figure 4E). These findings suggest that TAM inhibits copper-induced hepatic cuproptosis and effectively reinstates TCA cycle metabolic homeostasis.

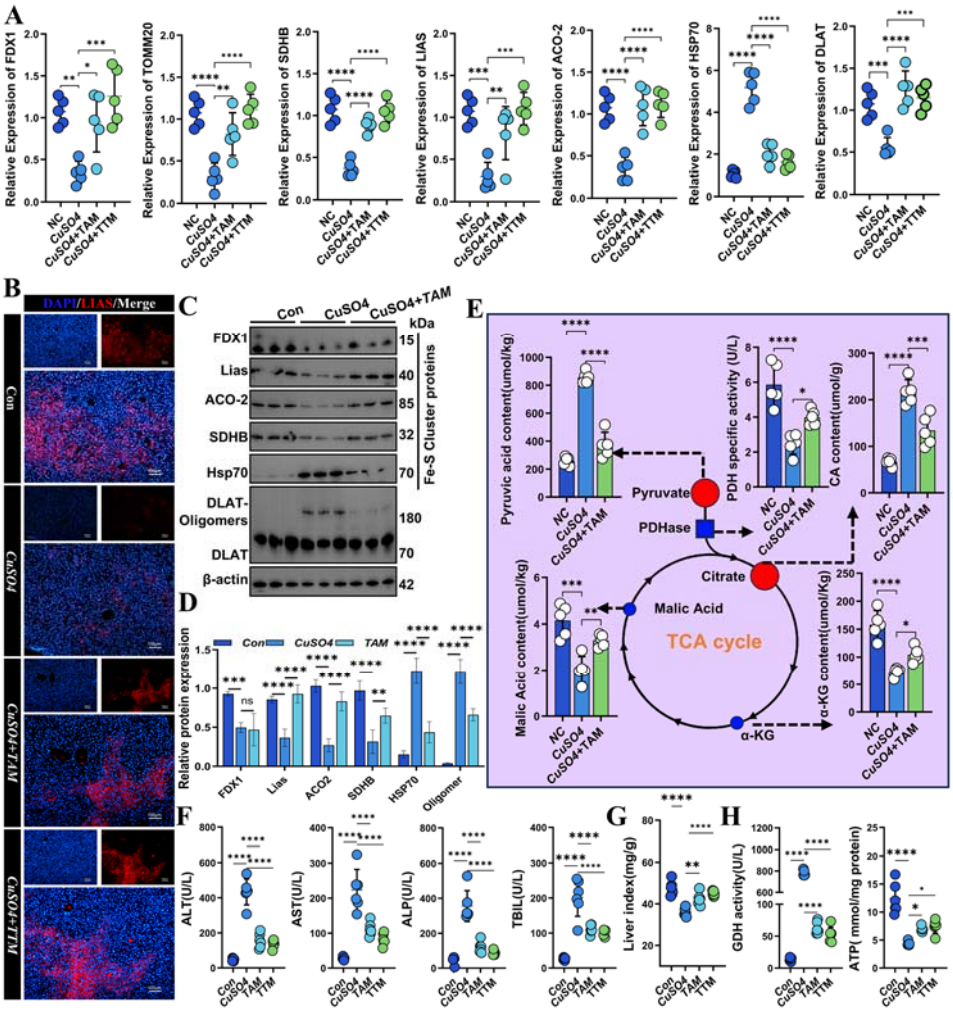


Figure 4. TAM attenuates high-copper-induced hepatic metabolic dysregulation and hepatotoxicity by inhibiting cuproptosis. (A) qRT-PCR detection of cuproptosis-related gene mRNA expression in mouse liver, including *FDX1*, *TOMM20*, *SDHB*, *LIAS*, *ACO-2*, *HSP70* and *DLAT* (n = 5); (B) fluorescence imaging of LIAS expression in liver frozen sections from different treatment groups (LIAS-red, DAPI-blue; scale bar: 100 μm); (C-D) Western blot detection of Fe-S cluster proteins, HSP70 and DLAT oligomerization levels in mouse liver after high-copper exposure and TAM intervention; (E) colorimetric assays of key TCA cycle enzyme activities and metabolite levels in mouse liver (blue box: pyruvate dehydrogenase activity; red circles: pyruvate and citrate; blue circles: α-ketoglutarate and malate), visualized on a TCA cycle diagram (n = 5); (F) comparison of serum AST, ALT, ALP and TBIL between TTM- and TAM-treated mice (n = 6); (G) comparison of liver index between TTM- and TAM-treated mice (n = 6); (H) comparison of serum GLDH and hepatic ATP between TTM- and TAM-treated mice (n = 6). Data are presented as mean ± SEM. (two-way ANOVA). * $P < 0.05$, ** $P < 0.01$, *** $P < 0.001$, **** $P < 0.0001$。

Further examinations demonstrated that, like the cuproptosis inhibitor TTM, TAM significantly improved liver function in copper-overloaded mice, as reflected by reduced serum levels of AST, ALT, ALP, and TBIL (Figure 4F). Both TAM and TTM also reversed the reduction in liver mass caused by high copper exposure (Figure 4G). Additionally, serum glutamate dehydrogenase (GLDH) and hepatic adenosine triphosphate (ATP) serve as established markers of mitochondrial injury in the liver. We observed that high copper exposure exacerbated hepatic mitochondrial damage, whereas TAM treatment markedly attenuated the copper-induced elevation of serum GLDH and the concomitant decline in hepatic ATP (Figure 4H). Collectively, these data indicate that TAM alleviates high-copper-induced mitochondrial metabolic dysfunction and hepatotoxicity in the liver through inhibition of cuproptosis.

3.4. TAM Regulates LIAS Transcriptional Expression by Upregulating NR1I2

To explore the mechanism by which TAM alleviates liver toxicity induced by copper exposure, potential targets of TAM were predicted using the SwissTargetPrediction GeneCards, BATMAN, and CTD, databases. Intersection analysis via Venn diagram revealed that NR1I2 was identified as a common candidate target across all four databases (Figure 5A, Table S1). NR1I2 (PXR), a key transcription factor, activates genes involved in drug and endogenous compound metabolism [37, 38]. Experimental results demonstrated that TAM treatment significantly increased both mRNA and protein levels of NR1I2, an effect observed independently of $CuSO_4$ exposure (Figure 5B-E). Molecular docking analysis further indicated stable binding between TAM and NR1I2, with a Vina score of -8.3 (Figure 5F, Table S2).

Subsequently, the ChEA3 database was employed to predict potential transcription factors regulating a cuproptosis-related gene set. Results suggested NR1I2 may participate in transcriptional regulation of DPYD, DLAT, and LIAS (Figure 5G). Lipoic acid modification, a critical process in cuproptosis, is primarily governed by LIAS; downregulation of LIAS expression compromises the stability of this modification and promotes cuproptosis [18, 19, 30].

Using the JASPAR database, binding sites of NR1I2 in gene promoters were analyzed (Figure 5I). The binding capability of NR1I2 to the LIAS promoter was predicted via AlphaFold3, indicating stable binding (ipTM = 0.8, pTM = 0.64) (Figure 5J), which implies direct transcriptional regulation of LIAS by NR1I2. Dual-luciferase reporter assays further confirmed NR1I2-mediated transcriptional activation of LIAS. Importantly, TAM treatment further increased luciferase activity in cells co-transfected with pGL3-pLIAS and pEGFP-C3-NR1I2 (Figure 5K). Consistent with these findings, TAM significantly upregulated LIAS expression (Figure 5L-N). In summary, these findings indicate NR1I2 acts as an upstream transcriptional regulator of LIAS, and TAM promotes LIAS expression by upregulating NR1I2.

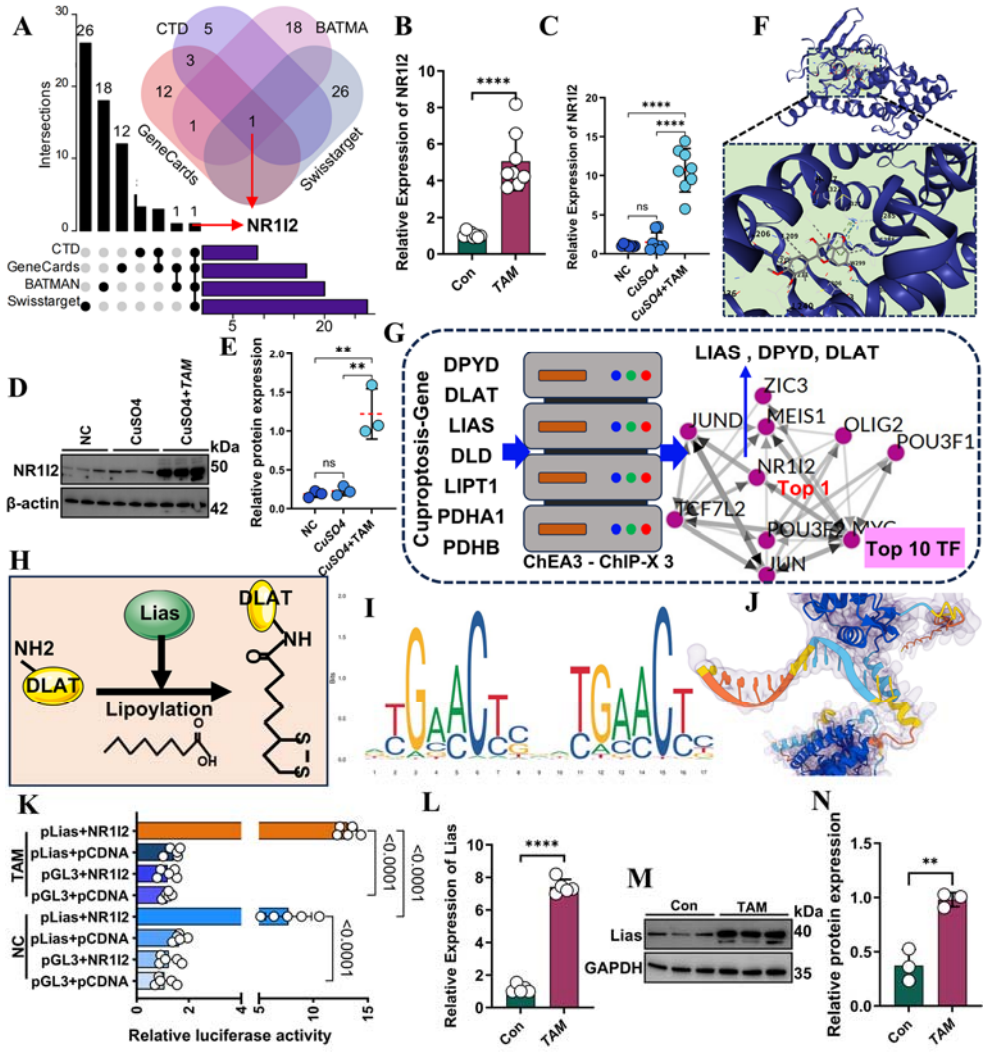


Figure 5. TAM regulates LIAS transcription by upregulating NR1I2. (A) Upset plot and Venn diagram analysis predicting putative TAM targets based on CTD, BATMAN, GeneCards and SwissTargetPrediction databases; (B-C) qRT-PCR detection of *NR1I2* mRNA levels in cells after TAM treatment under copper-exposed and non-exposed conditions (n = 8); (D-E) Western blot analysis of NR1I2 protein expression under high-copper exposure and TAM intervention; (F) visualization of the molecular docking binding mode between TAM and NR1I2 protein; (G) ChEA3 database prediction of the co-transcription factor network for a cuproptosis-related gene set; (H) schematic of LIAS-mediated protein lipoylation; (I) JASPAR database prediction of NR1I2 binding sites in the LIAS promoter region; (J) AlphaFold3-predicted conformation of NR1I2 binding to the LIAS promoter; (K) Dual-luciferase reporter assay: co-transfection of pGL3-pLIAS, pcDNA3.1-NR1I2 and pRL-TK into cells to validate NR1I2 transcriptional activation of the pLIAS (n = 5); (L) qRT-PCR detection of *LIAS* mRNA levels after TAM treatment (n = 5); (M-N) Western blot analysis of the effect of TAM treatment on LIAS protein expression. Data are presented as mean ± SEM. (two-way ANOVA). * $P < 0.05$, ** $P < 0.01$, *** $P < 0.001$, **** $P < 0.0001$.

3.5. Overexpression of NR1I2 Alleviates High Copper-Induced Oxidative Stress and Cuproptosis

To further validate the regulatory role of NR1I2 on LIAS expression, we cloned the CDS sequence of NR1I2 into the pEGFP-C3 vector and transfected it into HepG2 cells to establish an NR1I2-overexpressing cell line. These cells were then treated with high concentrations of $CuSO_4$ (Figure 6A). Immunoblot and qPCR analyses showed that NR1I2 levels remained unchanged in the empty vector group but were significantly elevated in the NR1I2-overexpressing group (Figure 6B-D). Consistent with this, NR1I2 overexpression also markedly increased LIAS expression (Figure 6C-D).

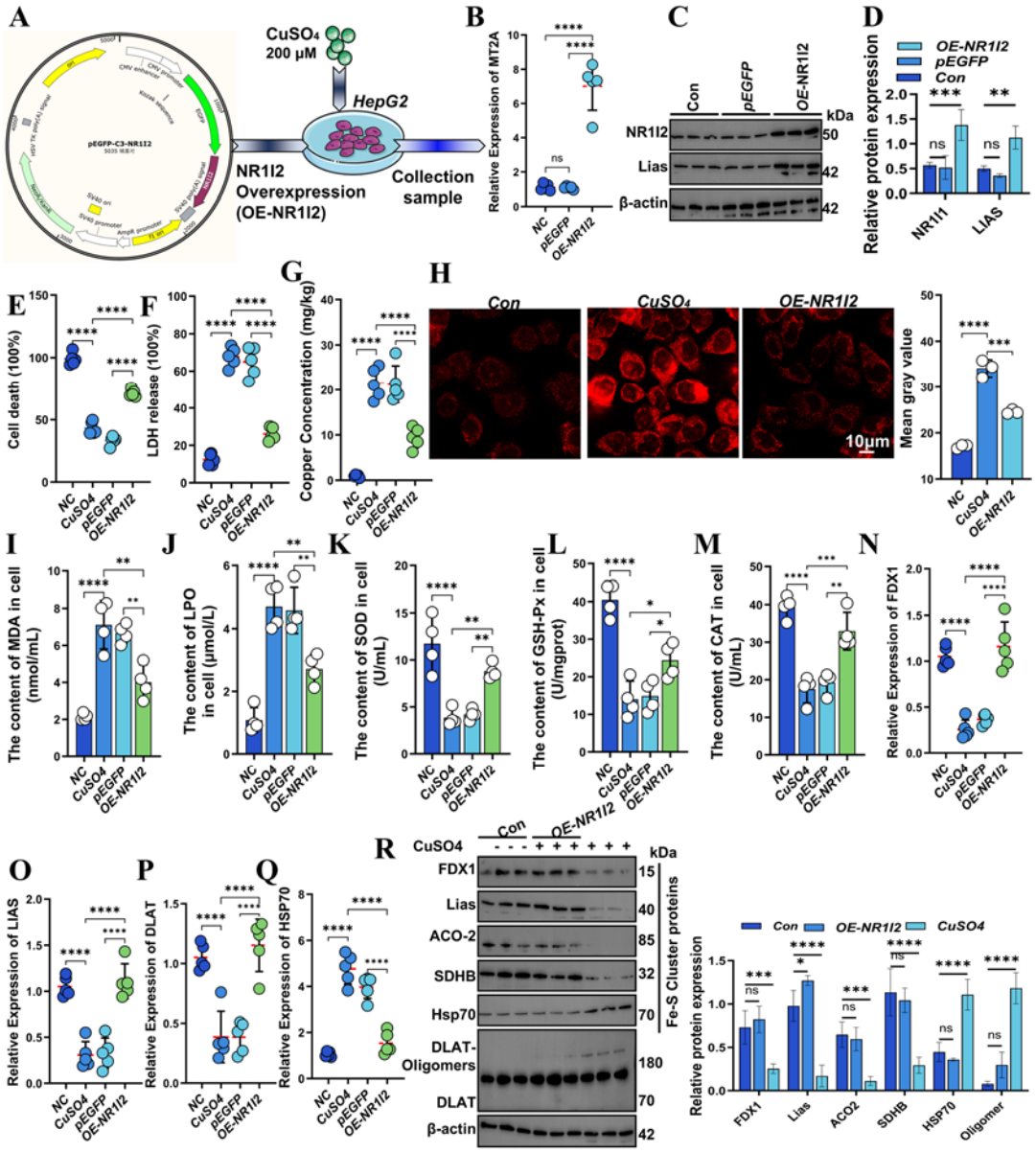


Figure 6. NR1I2 overexpression alleviates high-copper-induced oxidative stress and cuproptosis. (A) Experimental design for NR1I2 overexpression (OE-NR1I2) cells in the high-copper exposure model; (B) qRT-PCR detection of NR1I2 mRNA levels in OE-NR1I2 cells (n = 5); (C-D) Western blot analysis of NR1I2 and LIAS protein expression in OE-NR1I2 cells; (E-F) CCK-8 assay for cell viability (E) and LDH release rate (F) of OE-NR1I2 cells after high-copper exposure (n = 5); (G) ICP-MS measurement of intracellular copper content in OE-NR1I2 cells after high-copper exposure (n = 5); (H) fluorescence microscopy observation of intracellular ROS levels (n = 3); (I-M) oxidative stress indicators in OE-NR1I2 cells after high-copper exposure: MDA, LPO, SOD, GSH-Px and CAT (n = 4); (N-Q) qRT-PCR detection of cuproptosis-related gene mRNA expression in OE-NR1I2 cells after high-copper exposure, including *FDX1*, *LIAS*, *DLAT* and *HSP70* (n = 5); (R) Western blot analysis of Fe-S cluster proteins, HSP70 and DLAT oligomerization levels in OE-NR1I2 cells after high-copper exposure. Data are presented as mean ± SEM. (two-way ANOVA). * $P < 0.05$， ** $P < 0.01$， *** $P < 0.001$， **** $P < 0.0001$.

Further experiments revealed that NR1I2 overexpression significantly reduced high copper-induced cell death and LDH release (Figure 6E-F). Intracellular copper content was also markedly decreased in the overexpression group (Figure 6G). Moreover, NR1I2 overexpression lowered intracellular ROS levels (Figure 6H) and significantly attenuated copper overload-induced oxidative stress, as evidenced by decreased levels of MDA, SOD, and LPO, along with increased levels of CAT and GSH-Px (Figure 6I-M). Subsequent analysis indicated that NR1I2 overexpression counteracted the inhibitory effects of high copper on the mRNA expression of *FDX1*, *LIAS*, and *DLAT* (Figure 6N-Q). More importantly, overexpressing

NR1I2 prevented the loss of Fe-S cluster proteins and inhibited DLAT aggregation induced by copper overload. Together, these results demonstrate that NR1I2 overexpression alone can alleviate copper-induced oxidative stress and cuproptosis.

3.6. TAM Alleviates Liver Injury Through the Gut-Liver Axis

Previous studies have demonstrated that copper exposure induces hepatic injury through disruption of gut microbial composition and function [39, 40] To evaluate the regulatory role of TAM on the gut microbiota in this process, we compared the diversity and composition of the gut microbiota in mice from the copper-exposed group and the TAM-treated group. PCoA revealed separation in community structure between the two groups, indicating significant differences in composition (Figure7A). Based on FAPROTAX functional annotation, TAM treatment reduced the enrichment of microbial groups associated with "human_pathogens" following copper exposure (Figure7B). Combining species abundance differences, we constructed a phylogenetic tree of differential microbiota to visually display changes in relative species abundances between groups (Figure7C). At the genus level, TAM significantly increased the abundance of the *Lactobacillus* genus after copper exposure (Figure7D). LEfSe analysis further identified *Lactobacillus_johnsonii* as significantly enriched in the TAM group (Figure7E-F). The constructed differential microbiota correlation network showed that *Lactobacillus_johnsonii* occupied a key node in the network, suggesting it may play a central role in community homeostasis (Figure7G).

Differential microbiota PICRUSt2 functional potential analysis indicated that copper exposure enriched microbial functions in TCA cycle pathways related to cuproptosis, as well as inflammation-related Arachidonic acid metabolism and NOD-like receptor signaling pathway (Figure7H). Consistent with these findings, KEGG and GO enrichment analyses of DEGs identified by transcriptomic analysis revealed that TAM-downregulated genes were robustly enriched in inflammatory pathways, including the NOD-like receptor, Toll-like receptor, and NF-κB signaling pathways (Figure8A-B). Therefore, we examined the activity of the TLR4/NF-κB pathway in the liver. The results showed that copper exposure activated TLR4/NF-κB signaling, while TAM significantly inhibited the activation of this pathway (Figure8C). Accordingly, TAM treatment reduced the expression of pro-inflammatory cytokines TNF-α and IL-1β in the liver (Figure8D-F).

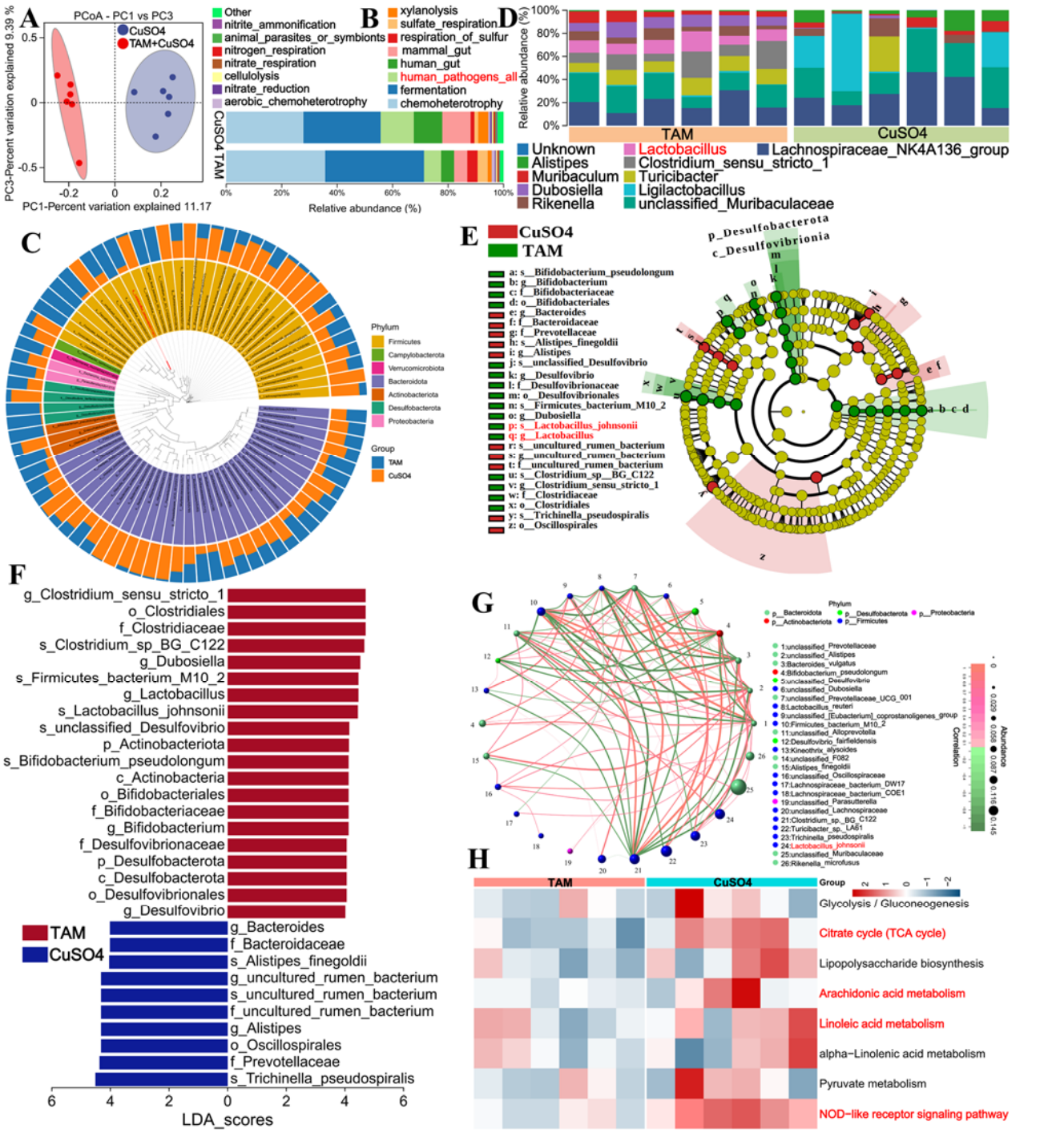


Figure 7. Diversity analysis of gut microbiota in mice exposed to high copper. (A) PCoA analysis based on Bray-Curtis distance showing differences in microbial communities among groups and samples; (B) differential microbiota FAPROTAX functional annotation; (C) selection of the top-80 high-abundance feature sequences at the OTU/ASV level for multiple sequence alignment and phylogenetic tree construction; (D) stacked bar chart of genus-level relative abundances; (E-F) intergroup LEfSe differential analysis: (E) cladogram showing significantly enriched taxa from phylum to species; (F) LDA score distribution bar chart; (G) microbial co-occurrence network analysis based on Spearman rank correlation; (H) PICRUSt2 functional prediction comparing metabolic functions of the gut microbiota across groups, emphasizing TCA cycle and inflammation-related pathways.

To explore the association between specific bacterial strains and liver injury, we conducted correlation analysis between the top 10 abundant microbiota and serum liver injury indicators (AST, ALT). The results indicated that *Lactobacillus_johnsonii* was significantly negatively correlated with AST and ALT (r^2=-0.86, and -0.91), suggesting that increased abundance of this strain is associated with improved liver function

(Figure8G). In summary, TAM may alleviate copper exposure-induced liver injury via the gut-liver axis by selectively enriching *Lactobacillus_johnsonii* and inhibiting inflammation-related pathways.

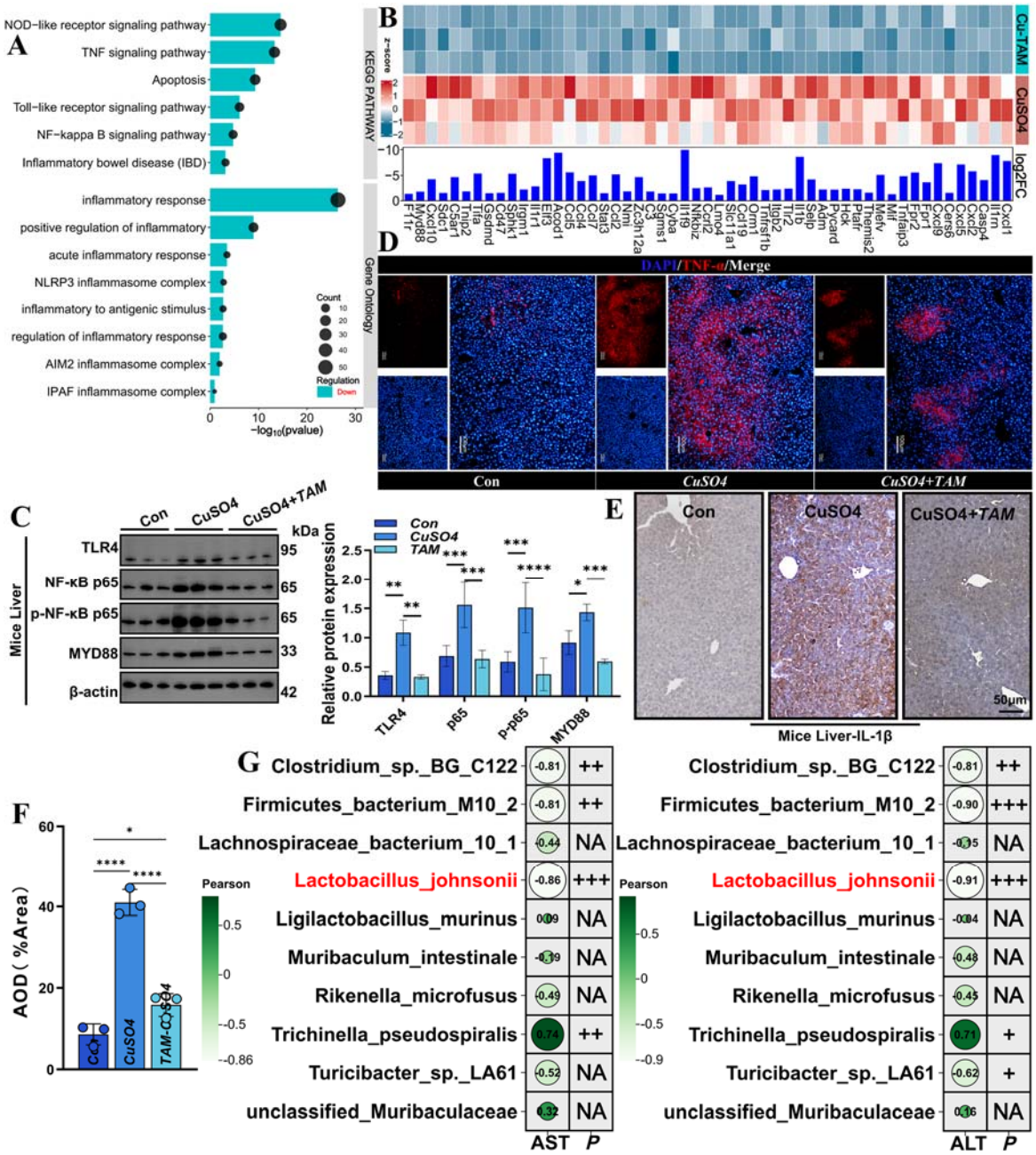


Figure 8. TAM attenuates high-copper-induced liver injury via the gut-liver axis. (A) KEGG and GO enrichment analyses of differential genes between high-copper and TAM intervention groups (inflammation-related pathways); (B) RNA-seq hierarchical clustering showing inflammation-related differential gene expression profiles after high-copper exposure and TAM intervention, including IL-1B, GSDMD, and members of the CCL and CXCL families; (C) Western blot detection of key proteins of the hepatic TLR4/NF-κB pathway (TLR4, NF-κB, p-NF-κB, MyD88); (D) fluorescence imaging of TNF-α in liver frozen sections (red: TNF-α, blue: DAPI; scale bar: 100 μm); (E-F) immunohistochemical detection of IL-1β in liver sections (scale bar: 50 μm); (G) Spearman correlation heatmap between the top-10 abundant gut microbiota genera and liver injury markers (AST, ALT) (+ P <0.05, ++ P <0.01, +++ P <0.001). Data are presented as mean ± SEM. (two-way ANOVA). * P < 0.05， ** P < 0.01， *** P < 0.001， **** P < 0.0001。

4. Discussion

This study, utilizing both *in vivo* and *in vitro* models of copper overload, confirms the pivotal role of cuproptosis in copper-induced toxicity. We found that TAM, as a natural flavonoid, alleviates hepatic

damage not only by directly chelating excess copper but also by activating the NR1I2–LIAS pathway. Through this dual action, TAM cooperatively suppresses cuproptosis, helps restore TCA cycle metabolic homeostasis, and reduces inflammation. In addition, TAM reshaped the gut microbiota, enriching beneficial *Lactobacillus*, which via the gut–liver axis contributed to the inhibition of NF-κB–mediated hepatic inflammatory responses.

While the metal-chelating and antioxidant properties of plant-derived flavonoids like TAM are well-documented in food chemistry [20, 21, 27] their capacity to modulate copper-dependent cell death has been largely unexplored. Our findings indicate that the hepatoprotective effects of TAM extend beyond a mere reduction in free copper load when compared with the classic copper chelator TTM. TAM acts at the transcriptional level by activating NR1I2, which in turn upregulates LIAS. NR1I2 is traditionally recognized for its role in xenobiotic metabolism [37, 38]; identifying it as a direct regulator of LIAS represents a paradigm shift. LIAS is required for the lipoylation of mitochondrial enzymes (such as DLAT) and is crucial for resisting cuproptosis [37, 38]. Our data suggest that NR1I2 binds to the LIAS promoter and drives its expression, thereby preserving DLAT oligomerization and maintaining Fe–S cluster proteins. Notably, simply overexpressing NR1I2 was sufficient to attenuate copper-induced cell death. Thus, the NR1I2–LIAS axis appears to be a critical node in preventing cuproptosis by sustaining protein lipoylation. It is important to recognize that FDX1 and LIAS may play dual roles in cuproptosis. During the initiation phase, they function as essential upstream factors required to establish copper sensitivity. Under sustained copper overload, however, the observed decline in their protein levels represents a hallmark of cuproptosis. Accordingly, the restoration of FDX1 and LIAS expression following TAM treatment should not be interpreted in isolation; it must be contextualized alongside concurrent findings namely, reduced DLAT oligomerization, preserved Fe-S cluster proteins, and attenuation of metabolic disruption and cellular injury. This mechanism sets TAM apart from structurally related flavonoids such as quercetin, which primarily act as copper chelators or antioxidants and are not known to influence the NR1I2–LIAS pathway [20, 21]. Therefore, TAM is more appropriately defined as a dietary flavonoid that combines nutritional intervention with mechanistic activity, rather than as a conventional single-target pharmacological chelator. Nevertheless, a comparative assessment of its efficacy relative to clinical copper-chelating agents must still be conducted in models that more closely recapitulate the disease context.

The discovery of the NR1I2–LIAS axis challenges the prevailing view that copper-induced cell death is driven solely by FDX1-mediated Cu^{2+} reduction and the subsequent aggregation of lipoylated proteins [15-17]. Instead, our data support a model where transcriptional support of LIAS by dietary bioactive compounds serves as a crucial defense against cuproptosis. This notion is consistent with studies showing that lipoic acid supplementation can alleviate copper toxicity, although the underlying regulatory mechanism had not been defined previously.

Beyond intracellular mechanisms, this study further delineates an ancillary role of the gut–liver axis in copper-induced liver injury and in the protective effects conferred by TAM. Excess dietary copper is known

to disrupt gut microbiota composition and promote intestinal and systemic inflammation [39, 40]. *Lactobacillus johnsonii*, in particular, enhances intestinal barrier function and reduces inflammation, but is reported to be depleted under high-copper exposure [41, 42]. Consistently, we observed that high-copper feeding nearly eradicated *L. johnsonii* in the mouse gut; notably, TAM treatment remodeled the gut microbiome by increasing *L. johnsonii* abundance and consequently attenuating NF-κB–mediated hepatic inflammation via the gut–liver axis. Moreover, we found a significant inverse correlation between *L. johnsonii* abundance and liver injury markers (serum AST/ALT), in line with reports that Lactobacillus species mitigate liver injury by inhibiting TLR4/NF-κB signaling [43, 44]. Compared with prior descriptive microbiome studies in metal toxicity [39], our findings connect specific microbial changes with liver protection However, regarding the gut–liver axis, we interpret these results primarily as correlative evidence related to the protective effects of TAM. The current data suggest that TAM-induced microbiota remodeling may reduce pro-inflammatory signals transmitted from the intestine to the liver, thereby aligning with the observed inhibition of NF-κB signaling. Together, these findings raise the possibility that strategies aimed at enriching beneficial gut bacteria, such as probiotic intervention, may enhance protection against dietary copper overload.

Although consistent evidence emerged from both mouse models and HepG2 cells, it should be noted that HepG2 is a hepatocellular carcinoma line whose metabolic profile may diverge from that of primary hepatocytes; future studies should employ primary human hepatocytes and hepatic organoids. Second, this study provides evidence for direct regulation of LIAS by NR1I2 using dual-luciferase reporter assays and molecular docking, but the computational predictions of NR1I2 binding should be further validated by experiments such as CUT&Tag. Finally, the contribution of *L. johnsonii* to TAM's protective effects needs further verification. This could be addressed by supplementing *L. johnsonii* as a probiotic or by conducting experiments in germ-free or antibiotic-treated mice. Under the exposure conditions examined here, cuproptosis constitutes the principal mode of cell death; in physiological contexts involving varying copper concentrations, exposure durations, or chronic exposure models, other death pathways may play secondary roles, a possibility that warrants further investigation.

In summary, our study establishes that cuproptosis is a critical mechanism driving copper-related liver injury and identifies NR1I2 as a key regulator mediating an LIAS-dependent copper detoxification response. By simultaneously modulating cellular copper homeostasis and the gut microbiome, TAM proves to be an effective natural agent against copper toxicity. This plant flavonoid could be developed as a functional food ingredient or food additive to improve safety under high-copper dietary conditions. Future work should explore the practical dietary application of TAM and consider microbiome-focused interventions (e.g., probiotic supplementation) as strategies to mitigate the effects of excessive dietary copper exposure.

Data Availability Statement

The data that support the findings of this study are available in the Supporting Information of this article. Additional file1: Table S1. The database predicted the potential targets of TAM. Table S2 Molecular

docking scores of TAM and NR1I2. Figure S1 Uncropped versions of all gel images-1 (Related to Figures 3, 4, and 5). Figure S2 Uncropped versions of all gel images-2 (Related to Figures 6, and 8).

Declaration of Competing Interest

The authors declare no competing financial interest.

Funding

This work was supported by the National Natural Science Foundation of China (Grant Nos. 32460868, 31960692, and 31660704).

Acknowledgments

We thank all project contributors for their efforts and Ms. Hongxu Yao (Yunnan Agricultural University) for her assistance with data analysis and organization.

Declaration of generative AI use

During the writing of this thesis, we used [ChatGPT] for [language translation and text polishing]. After using this tool, we have conducted necessary reviews and revisions of the content, and we take full responsibility for the final content of the published article.

References

1. Kim B, Nevitt T, Thiele D: Mechanisms for copper acquisition, distribution and regulation. *Nature chemical biology* 2008, 4(3):176-185.
2. Inesi G: Molecular features of copper binding proteins involved in copper homeostasis. *IUBMB life* 2017, 69(4):211-217.
3. Zhong L, Wang L, Xu L, Liu Q, Jiang L, Zhi Y, Lu W, Zhou P: The role of NOS-mediated ROS accumulation in an early phase Cu-induced acute cytotoxicity in MCF-7 cells. *Biometals : an international journal on the role of metal ions in biology, biochemistry, and medicine* 2015, 28(1):113-122.
4. Cai H, Cheng X, Wang XP: ATP7B gene therapy of autologous reprogrammed hepatocytes alleviates copper accumulation in a mouse model of Wilson's disease. *Hepatology* 2022, 76(4):1046-1057.
5. Kirk FT, Munk DE, Swenson ES, Quicquaro AM, Vendelbo MH, Larsen A, Schilsky ML, Ott P, Sandahl TD: Effects of tetrathiomolybdate on copper metabolism in healthy volunteers and in patients with Wilson disease. *J Hepatol* 2024, 80(4):586-595.
6. Liu T, Liu Y, Zhang F, Gao Y: Copper homeostasis dysregulation promoting cell damage and the association with liver diseases. *Chin Med J (Engl)* 2023, 136(14):1653-1662.
7. Lutsenko S, Bhattacharjee A, Hubbard A: Copper handling machinery of the brain. *Metallomics : integrated biometal science* 2010, 2(9):596-608.
8. Zhang Y, Dong Z, Yang H, Liang X, Zhang S, Li X, Wan D, Yin Y: Effects of dose and duration of dietary copper administration on hepatic lipid peroxidation and ultrastructure alteration in piglets' model. *J Trace Elem Med Biol* 2020, 61:126561.
9. Li M, Tang S, Velkov T, Shen J, Dai C: Copper exposure induces mitochondrial dysfunction and hepatotoxicity via the induction of oxidative stress and PERK/ATF4 -mediated endoplasmic reticulum stress. *Environ Pollut* 2024, 352:124145.
10. Tsvetkov P, Coy S, Petrova B, Dreishpoon M, Verma A, Abdusamad M, Rossen J, Joesch-Cohen L, Humeidi R, Spangler R *et al*: Copper induces cell death by targeting lipoylated TCA cycle proteins. *Science (New York, NY)* 2022, 375(6586):1254-1261.
11. Daolin T, Guido K, Rui K: Targeting cuproplasia and cuproptosis in cancer. *Nature Reviews Clinical Oncology* 2024.

12. Sun L, Zhang Y, Yang B, Sun S, Zhang P, Luo Z, Feng T, Cui Z, Zhu T, Li Y *et al*: Lactylation of METTL16 promotes cuproptosis via m6A-modification on FDX1 mRNA in gastric cancer. *Nature Communications* 2023, 14(1):6523.
13. Chen N, Guo L, Wang L, Dai S, Zhu X, Wang E: Sleep fragmentation exacerbates myocardial ischemia–reperfusion injury by promoting copper overload in cardiomyocytes. *Nature Communications* 2024, 15(1):3834.
14. Jiaming X, Yong Y, Yibo G, Jie H: Cuproptosis: mechanisms and links with cancers. *Molecular Cancer* 2023.
15. Li Y, Ma J, Wang R, Luo Y, Zheng S, Wang X: Zinc transporter 1 functions in copper uptake and cuproptosis. *Cell Metabolism* 2024, 36(9):2118-2129.e2116.
16. Lei G, Sun M, Cheng J, Ye R, Lu Z, Horbath A, Huo D, Wu S, Alapati A, Aggarwal S *et al*: Radiotherapy promotes cuproptosis and synergizes with cuproptosis inducers to overcome tumor radioresistance. *Cancer cell* 2025.
17. Dang D, Deogharkar A, McKolay J, Smith KS, Panwalkar P, Hoffman S, Tian W, Ji S, Azambuja AP, Natarajan SK *et al*: Isocitrate dehydrogenase 1 primes group-3 medulloblastomas for cuproptosis. *Cancer cell*.
18. Wang Y, Zhang L, Zhou F: Cuproptosis: a new form of programmed cell death. *Cellular & molecular immunology* 2022, 19(8):867-868.
19. Lin J, Yin Y, Cao J, Zhang Y, Chen J, Chen R, Zou B, Huang C, Lv Y, Xu S *et al*: NUDT21 lactylation reprograms alternative polyadenylation to promote cuproptosis resistance. *Cell Discov* 2025, 11(1):52.
20. Lee SH, Shin MK, Sung JS: Tamarixetin Protects Chondrocytes against IL-1β-Induced Osteoarthritis Phenotype by Inhibiting NF-κB and Activating Nrf2 Signaling. *Antioxidants (Basel)* 2024, 13(10).
21. Lomozová Z, Catapano MC, Hrubša M, Karlíčková J, Macáková K, Kučera R, Mladěnka P: Chelation of Iron and Copper by Quercetin B-Ring Methyl Metabolites, Isorhamnetin and Tamarixetin, and Their Effect on Metal-Based Fenton Chemistry. *Journal of Agricultural and Food Chemistry* 2021, 69(21):5926-5937.
22. Sultanova N, Makhmoor T, Abilov ZA, Parween Z, Omurkamzinova VB, ur-Rahman A, Choudhary MI: Antioxidant and antimicrobial activities of Tamarix ramosissima. *Journal of ethnopharmacology* 2001, 78(2-3):201-205.
23. Bedir E, Tatli, II, Khan RA, Zhao J, Takamatsu S, Walker LA, Goldman P, Khan IA: Biologically active secondary metabolites from Ginkgo biloba. *J Agric Food Chem* 2002, 50(11):3150-3155.
24. Fan C, Li Y, Yang H, Cui Y, Wang H, Zhou H, Zhang J, Du B, Zhai Q, Wu D *et al*: Tamarixetin protects against cardiac hypertrophy via inhibiting NFAT and AKT pathway. *Journal of molecular histology* 2019, 50(4):343-354.
25. Lee S-H, Shin MK, Sung J-S: Tamarixetin Protects Chondrocytes against IL-1β-Induced Osteoarthritis Phenotype by Inhibiting NF-κB and Activating Nrf2 Signaling. *Antioxidants* 2024, 13(10):1166.
26. Park HJ, Lee SJ, Cho J, Gharbi A, Han HD, Kang TH, Kim Y, Lee Y, Park WS, Jung ID *et al*: Tamarixetin Exhibits Anti-inflammatory Activity and Prevents Bacterial Sepsis by Increasing IL-10 Production. *Journal of natural products* 2018, 81(6):1435-1443.
27. Ijaz MU, Khalil M, Hamza A, Khatoon A: Attenuative effects of tamarixetin against polystyrene microplastics-induced hepatotoxicity in rats by regulation of Nrf-2/Keap-1 pathway. *Cell biochemistry and function* 2023, 41(8):1451-1461.
28. Wu H, Guo H, Liu H, Cui H, Fang J, Zuo Z, Deng J, Li Y, Wang X, Zhao L: Copper sulfate-induced endoplasmic reticulum stress promotes hepatic apoptosis by activating CHOP, JNK and caspase-12 signaling pathways. *Ecotoxicology and Environmental Safety* 2020, 191:110236.
29. Yang Y, Wang F, Fang M, Yao X, Xu L, Liu Y, Liu Y, Liang D, Zeng K, Li N *et al*: Tamarixetin ameliorates cerebral ischemia-reperfusion injury via suppressing nicotinamide adenine dinucleotide phosphate oxidase 2/nucleotide-binding oligomerization domain like receptor family pyrin domain-containing 3 inflammasome activation. *Phytotherapy research : PTR* 2024, 38(8):4286-4306.
30. Peter T, Shannon C, Boryana P, Margaret D, Ana V, Mai A, Jordan R, Lena J-C, Ranad H, Ryan DS *et al*: Copper induces cell death by targeting lipoylated TCA cycle proteins. *Science* 2022.
31. Xiaowei W, Athanasia S, Huajun W, Brian S: PrimerBank: a PCR primer database for quantitative gene expression analysis, 2012 update. *Nucleic Acids Research* 2011.
32. Athanasia S, Xiaowei W, Huajun W, Brian S: PrimerBank: a resource of human and mouse PCR primer pairs for gene expression detection and quantification. *Nucleic Acids Research* 2009.

33. Keenan AB, Torre D, Lachmann A, Leong AK, Wojciechowicz ML, Utti V, Jagodnik KM, Kropiwnicki E, Wang Z, Ma'ayan A: ChEA3: transcription factor enrichment analysis by orthogonal omics integration. *Nucleic Acids Research* 2019, 47(W1):W212-W224.
34. Liu Y, Yang X, Gan J, Chen S, Xiao Z-X, Cao Y: CB-Dock2: improved protein–ligand blind docking by integrating cavity detection, docking and homologous template fitting. *Nucleic Acids Research* 2022, 50(W1):W159-W164.
35. Gaetke LM, Chow CK: Copper toxicity, oxidative stress, and antioxidant nutrients. *Toxicology* 2003, 189(1-2):147-163.
36. Su-Ran L, Lin-Lin B, Lulu C: Cuproptosis: lipoylated TCA cycle proteins-mediated novel cell death pathway. *Signal Transduction and Targeted Therapy* 2022.
37. Xie W, Barwick JL, Simon CM, Pierce AM, Safe S, Blumberg B, Guzelian PS, Evans RM: Reciprocal activation of xenobiotic response genes by nuclear receptors SXR/PXR and CAR. *Genes & development* 2000, 14(23):3014-3023.
38. Watkins RE, Maglich JM, Moore LB, Wisely GB, Noble SM, Davis-Searles PR, Lambert MH, Kliewer SA, Redinbo MR: 2.1 A crystal structure of human PXR in complex with the St. John's wort compound hyperforin. *Biochemistry* 2003, 42(6):1430-1438.
39. Dai J, Yang X, Yuan Y, Jia Y, Liu G, Lin N, Xiao H, Zhang L, Chen J: Toxicity, gut microbiota and metabolome effects after copper exposure during early life in SD rats. *Toxicology* 2020, 433-434:152395.
40. Gu T, Kong M, Duan M, Chen L, Tian Y, Xu W, Zeng T, Lu L: Cu exposure induces liver inflammation via regulating gut microbiota/LPS/liver TLR4 signaling axis. *Ecotoxicol Environ Saf* 2024, 278:116430.
41. Wen Y, Yang L, Wang Z, Liu X, Gao M, Zhang Y, Wang J, He P: Blocked conversion of Lactobacillus johnsonii derived acetate to butyrate mediates copper-induced epithelial barrier damage in a pig model. *Microbiome* 2023, 11(1):218.
42. Jia DJ, Wang QW, Hu YY, He JM, Ge QW, Qi YD, Chen LY, Zhang Y, Fan LN, Lin YF *et al*: Lactobacillus johnsonii alleviates colitis by TLR1/2-STAT3 mediated CD206 + macrophages IL-10 activation. *Gut Microbes* 2022, 14(1):2145843.
43. L H, Z Z, C D, C W, Y Z, G Y, L G, C N, J X, S L: Lactobacillus plantarum C88 protects against aflatoxin B 1 -induced liver injury in mice via inhibition of NF-κB-mediated inflammatory responses and excessive apoptosis. *BMC microbiology* 2019, 19(1):170.
44. H L, J S, L Z, J G, F L, G H, B L: Lactobacillus plantarum KLDS1.0344 and Lactobacillus acidophilus KLDS1.0901 Mixture Prevents Chronic Alcoholic Liver Injury in Mice by Protecting the Intestinal Barrier and Regulating Gut Microbiota and Liver-Related Pathways. *Journal of agricultural and food chemistry* 2021, 69(1):183-197.